Spectral Analysis of Cytochrome *c*: Effect of Heme Conformation, Axial Ligand, Peripheral Substituents, and Local Electric Fields

Ivan Rasnik,[†] Kim A. Sharp,[†] James A. Fee,[‡] and Jane M. Vanderkooi*[,†]

Johnson Research Foundation, Department of Biochemistry and Biophysics, University of Pennsylvania, School of Medicine, Philadelphia Pennsylvania 19104-6059, and Department of Biology, Room 2218 Bonner Hall, University of California at San Diego, 9500 Gilman Drive, La Jolla, CA 92093-0368

Received: July 26, 2000

We present in this work low-temperature visible absorption spectra for recombinant *Thermus thermophilus* cytochrome c_{552}. The Q-band presents a remarkable splitting at low temperature. We performed quantum chemical calculations to evaluate quantitatively the effect of heme conformation, axial ligand, peripheral substituents and local electric fields on the electronic spectra. In an attempt to find correlation between protein structure and spectral splitting, we carried out the same calculations on three other cytochrome *c*'s: horse heart, tuna heart, and yeast. The quantum chemical calculations were performed at the INDO level with extensive configuration interaction. The electric field at the heme pocket was included in the calculations through a set of point charges fitting the actual electric field. The results obtained show clearly that all mentioned effects contribute to the observed spectral splitting in a complex nonadditive way.

I. Introduction

The UV−vis absorption spectra of heme proteins have been object of extensive research for many years. Their spectra are associated with the metalloporphyrin macrocycle present in all these proteins, which plays a central role in their specific biological function: oxygen transport, one-electron-transfer agents and irreversible covalent transformations of substrates.[1] The porphyrin macrocycle and axial ligands have direct effects on the different possible iron spin and oxidation states,[2] that make possible the variety of physicochemical processes in which the heme group is involved. At the same time, the porphyrin conformation and axial ligand geometry are strongly influenced by the protein environment, making the whole system an interesting subject for the study of biological function−structure relationship.

The absorption spectra of the heme group can provide important information on the electronic structure of the metalloporphyrin complex and its environment. Although the essential features of the spectra are well understood,[3] a complete quantitative correlation with all variables affecting the spectra is still lacking.

Fe(II)−porphyrin complexes, in the presence of strong axial ligands, present spectra with characteristics typical of closed shell metalloporphyrins.[4] The main features of these spectra are the Q(0,0) band in the visible region (∼580 nm), of electronic origin, the Q(0,1) (∼520 nm) band, associated with the Q(0,0) band electronic transitions but involving also vibrational excitations, and the B or Soret band, a much more intense band in the UV region (∼420 nm) of electronic origin. It is well-known that the Q(0,0) band in some low-spin heme proteins show splitting in the range of 50−200 cm^{-1} that becomes more resolved as the temperature is lowered.[5−12] This splitting can be viewed as an effect of the "symmetry lowering environment" on the metalloporphyrin complex; a departure from the square symmetry (D_{4h}) should induce this splitting, but the amount of splitting cannot be predicted with symmetry arguments. Experimentally, it has been shown that the protein structure, which determines the heme pocket environment, has direct effect on the Q(0,0) band splitting.[5,8,9,13−15] Various interpretations have been proposed to account for the Q-band splitting[7,10,16] in a qualitative way, based on the concept of low symmetry environment.

In a series of two papers,[15,17] Manas et al. presented the first systematic approach to include the effects of environment in electronic spectra calculations for cytochrome *c*'s. These works show the importance of the electric field effects on the heme spectra. In the first of these papers the effect is considered as a perturbation on a five-level model (in an extension of Gouterman's four level model[18]). These results showed that macrocycle conformation and electrostatic external field combined can induce spectral splitting of the order of magnitude that is experimentally observed. Moreover, they suggest that the overall effect will depend strongly on the electrostatic field symmetry, giving a clear physical picture of the effects involved in the Q-band splitting. Because of the approximations involved in this kind of approach, the method is not well suited for exact quantitative calculations. In the second paper of this series, the electrostatic field was included in the quantum chemical spectra calculation for Zn substituted cytochrome *c* proteins. Because of the closed d-electron shell of Zn, the effect of axial ligands is of minor importance relative to the iron proteins. The propionic acids attached to the macrocycle were treated as external perturbation through their electric field.

In this paper, we are extending the previous work. We present experimental results of the visible absorption spectra of cytochrome c_{552}. The relatively large Q(0,0) splitting that this protein exhibits motivates us to look for structural factors that could determine such splitting. As mentioned above, no previous works on spectral splitting calculations for heme-proteins include

* To whom correspondence should be addressed. Phone: 25-898-8783. E-mail: vanderko@mail.med.upenn.edu.
[†] University of Pennsylvania.
[‡] University of California at San Diego.

10.1021/jp002656k CCC: $20.00
Published on Web 12/09/2000

all external effects at the same level of approximation. We performed quantum chemical calculations for this purpose for *Thermus* cytochrome c_{552} and three other cytochromes *c* with known 3-D structure, namely the cytochrome *c*'s from horse, yeast and tuna. This permitted us to study systematically the effects of axial ligands, ring conformation, peripheral substituents and electrostatic field.

II. Materials and Methods

Experimental Methods. Recombinant cytochrome c_{552} was prepared from *Escherichia coli* cells that had been engineered to express the chimeric *cya*A gene of *Thermus thermophilus* HB8[19] This recombinant material is identical in function and structure to native *Thermus* cytochrome c_{552} except that it is shorter by 2 amino acids at the N-terminus.[20,21] The lyophillized protein was dissolved in 10 mM phosphate buffer pH 7.0 that was diluted to 50 vol % with glycerol. The iron was reduced by addition of dithionite. The sample concentration was ~4 mM. A Hitachi U-300 UV−vis spectrophotometer was used to measure the spectra. The path length of the sample cell was 0.05 mm. Details of the cryostat are given by Manas et al.[17] The spectra were taken from high to low temperature, and the sample was allowed to equilibrate for about 10 min after the desired temperature was obtained.

Computational Modeling. Quantum chemical calculations on the heme group utilized the ZINDO/s semiempirical method developed and parametrized for spectroscopy by Zerner and coworkers[22−24] as implemented in the Cerius 2 software package (Molecular Simulations Inc., Sherrills Ford, NC). Singles configuration interactions was used in conjunction with the INDO1/s method to calculate optical spectra. Excitations from 59 occupied to 59 unoccupied molecular orbitals were included in the SCI calculation. The independence of the results on the number of orbitals included was checked by performing configuration interaction calculations with different number of orbitals. As our calculations are focused on the lowest electronic transitions, involving few orbitals near the highest occupied molecular orbital (HOMO) and lowest unoccupied molecular orbital (LUMO), a good description of the transitions is obtained with a relatively small number of molecular orbitals included in the configuration interaction calculation.

The electric field imposed on the heme group by the protein and solvent environment was simulated by a set of fixed point charges included in the ZINDO calculation. As the point charges enter in the Fock matrix as a Coulombic potential they do not add significant computation time and provide a simple way to introduce the external electric field in the quantum chemical calculations. For the results of this method to be meaningful the electric field in the heme pocket produced by the set of point charges must fit precisely the actual electric field in this region. To generate the set of point charges, we follow the method employed by Manas et al.[15] The electric field at the heme site is first calculated solving the Poisson−Boltzmann equation (eq 1) by finite difference (FDPB) using the software package DelPhi.[25−28]

$$\nabla[\epsilon(\vec{r})\ \nabla\phi(\vec{r})] - \kappa(\vec{r})^2\ \epsilon(\vec{r})\ \sinh[\phi(\vec{r})] = -4\pi\rho(\vec{r})/k_B T \quad (1)$$

where $\phi(\vec{r})$ is the electrostatic potential in units of $k_B T/e$ (k_B is the Boltzmann constant, *T* is the absolute temperature and *e* is the elementary charge unit), $\epsilon(\vec{r})$ is the dielectric constant, $\rho(\vec{r})$ is the fixed charge density (in units of e), and $\kappa(\vec{r})$ is the Debye−Hückel constant, which is proportional to the square root of the ionic strength: $\kappa(\vec{r})^2 = 8\pi e^2 I/\epsilon(\vec{r})k_B T$. A two dielectric model is used for the protein−solvent system, with the dielectric boundary defined by the molecular surface of the protein. A dielectric constant of 2 was used for the protein and a dielectric constant of 80 for the solvent, with an ionic strength of 0.1 M. The protein contributions to the electric field in the heme pocket can be considered as sum of the electric field of charged groups at the experimental pH and that of polar groups (zero net charge). A comparison between both contributions is described in detail in a previous work.[17] The results we present in this work include only the formal charge set, with contributions of the charged groups. Within this scheme the charge assignment was −0.5 to the OD1, OD2 and OE1, OE2 oxygens of the Asp and Glu residues, respectively. In addition a charge of +0.5 was assigned to the NH1 and NH2 nitrogens of Arg and +1.0 to the NZ lys nitrogen. In previous works, the heme propionates were treated as an external perturbation to the heme group through their electric field, assigning a charge of −0.5 to their oxygens. In this work we performed different calculations, including them at this same level or explicitly in the quantum mechanical calculation. The parameters used for the finite difference calculation were: grid dimensions 65 in each direction, corresponding to a scale of about 1.1 grids/Å, Debye−Hückel type boundary conditions, multigrid method of iteration combined with dielectric smoothing and charge anti-aliasing with a final convergence of value of 1×10^{-4} *kT*/e total residue error in the potential.

The potential and electric field in each atom of the heme group obtained in this way can be fitted by a set of *n* point charges of charge q_j and spatial coordinates r_j (equivalent to fitting the electrostatic potential and its gradient). Provided the number of point charges is greater than 4*m* (with *m* the number of atoms in the heme group) no unique solution exists for the set $(q_j,\vec{r}_j)$ and a single value decomposition routine can be used to solve the problem. The over-determination of the system is exploited in this way for numerical convenience, setting the coordinates of the point charges on a spherical shell of radius *R* that encloses the heme group. It should be noted that the method itself does not guarantee that the electrostatic potential and electric field in the surrounding region, where the molecular orbitals extend, fits the FDPB field. Because part of our calculations included explicitly the axial ligands and peripheral substituents of the porphyrin ring, the electric field had to be fitted in a more extended region of space with reduced symmetry than used in the Manas et al. work. Dependence of the results on the particular choice of point charge set was observed but the general trends in the calculated electric field effects on the spectra did not change, so we did not make any attempts to improve the algorithms used for those calculations. An alternative approach was used to compare these results. Given the charged residues in the protein as determined by the formal charge set described above, we include them as point charges directly in the quantum chemical calculation and set a constant dielectric screening for those charges as implemented in the ZINDO package (we performed tests varying this dielectric screening between 1 and 4). This is the more elemental approximation[29] to the actual electric field in the heme group, but as it does not involves intermediate steps, it constitutes a good reference calculation. Despite minor quantitative differences the same general trends were observed with this method.

Coordinates for the cytochrome *c* used in this work where taken from the entries 1HRC.PDB,[30] 5CYT.PDB,[31] 1YCC.PDB,[32] and 1DT1.PDB[19] of the Research Collaboratory for Structural Bioinformatics for horse heart (HH), tuna heart (TH),

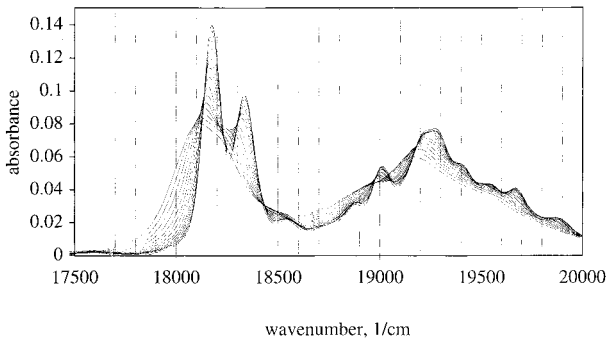

Figure 1. Absorption spectra for cytochrome c_{552} for different temperatures. Visible or Q(0,0) region. The spectra was recorded from higher (290 K) to lower temperature (10 K) in increments of 10 deg. The lower, least resolved spectra are for the higher temperature. Sample conditions given in Materials and Methods.

TABLE 1: Fe−N and Fe−S Distances As Obtained from the pdb Files, Root Mean Square of the Distance of the Atoms of the Macrocycle from Their Mean Plane, and Root Mean Square Deviation of the In-Plane Coordinates for the Macrocycle Atoms from a Reference Macrocycle, As Explained in the Text

	Fe−N (Å)	Fe−S (Å)	$\sqrt{\Sigma\Delta z^2}$ (Å)	$\sqrt{\Sigma\Delta x^2 + \Delta y^2}$ (Å)
C552	2.07	2.30	0.87	0.14
horse heart	2.04	2.32	1.06	0.26
tuna heart	1.98	2.31	0.76	0.19
yeast	1.99	2.35	0.89	0.25

TABLE 2: Spectral Splitting of the Q(0,0) Band

	ΔQ (cm^{-1})[a]	ΔQ (cm^{-1})[b]	ΔQ (cm^{-1})[c]	ΔQ (cm^{-1})[d]
C552	153	14.0	111.3	167.2
horse heart	119	91.7	30.9	62.6
tuna heart	104	61.0	99.0	148.6
yeast	80	322.8	280.2	183.2

[a] Experimental values. [b] Quantum chemical calculation, macrocycle conformation, and axial ligands orientation as obtained from the pdb files. The peripheral substituents were replaced by hydrogen. [c] Same as in footnote b, but including the peripheral substituents. This shows particullarly the effect of the propionates on the splitting. [d] Same as in footnote *c* including also the electrostatic field generated by the charged residues of the protein.

yeast (Y) cytochrome *c* and *Thermus* cytochrome c_{552}, respectively. The structure modifications necessary for the different quantum mechanical calculations c_{552} (as adding hydrogen, changing peripheral substituents) were performed with the Biopolymer module of the Insight II software package (Biosym Technologies, San Diego, CA).

III. Results and Discussion

Experimental Results. The experimental and theoretical results shown in this work are on Fe(II)−porphyrin. The experimental spectra for cytochrome c_{552} at different temperatures are shown in Figure 1. The essential features are those typical of hypsoporphyrin spectra,[4] indicating a closed d-electrons subshell for the Fe(II). At room temperature, the Q(0,0) band shows a shoulder that becomes more resolved as temperature goes down and the splitting in the spectrum reaches a relatively high value, as compared with other cytochrome *c* proteins (first column of Table 2), of 157 cm^{-1}. A similar observation with native *Thermus* cytochrome c_{552} was made earlier by Hon-Nami and Oshima.[33] An overall line width reduction and a small blueshift are also observed as temperature is decreased.

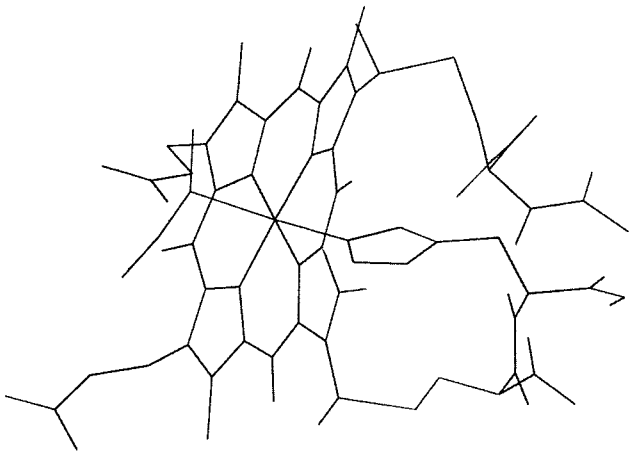

Figure 2. X-ray structure of cytochrome c_{552} in the region near the heme pocket. Note the rigid orientation of the axial histidine imposed by the covalent bonds.

Theoretical Calculations. As mentioned in the Introduction, the strong axial ligands present in all cytochromes *c* stabilize the low spin state, under these conditions the Q(0,0) band involves only pure $\pi \rightarrow \pi^*$ transitions, although the iron d-orbitals can affect this transition in an indirect way. In the D_{4h} symmetry metalloporphyrin complex the Q-band is associated with the highest occupied molecular orbitals, of symmetry a_{2u} and a_{1u} (accidentally quasi-degenerate), and the lowest unoccupied molecular orbitals of symmetry e_g. As the D_{4h} symmetry is broken the orbital degeneracy may break and the Q-band should split. In cytochrome *c*, the heme group is subject to perturbations that may produce an effective break of symmetry: structural constraints, axial ligands, nonsymmetric peripheral substituents and electrostatic field.

Axial Ligands. The axial ligands for Fe in these proteins are Histidine and Methionine. This asymmetric coordination can by itself break the symmetry (eliminating the plane of reflection), but a more important effect (as shown by our calculations) is the orientation of the histidine ring. In all our studied structures (and all cytochrome *c* X-ray structures that we know), the plane of the histidine ring adopts a conserved orientation, shown in Figure 2 for the cytochrome c_{552} structure. It is also possible to see in this figure that, because of the covalent bonding of two different atoms of the histidine ring to the protein, rotation along the N−Fe bond is highly improbable. To evaluate the effect of axial ligands on the spectra, we performed quantum chemical calculations on a planar symmetric porphyrin ring (bond lengths as in work by Edwards et al.[34]), with no peripheral substituents (hydrogen). We studied both symmetric substitution (two imidazole ligands, with their cycles planes parallel to each other and oriented as His in the studied structures) and asymmetric substitution (one imidazole ligand and $S(CH_3)_2$ to model the methionine ligand). The Fe−N and Fe−S bond lengths were taken as the mean value of the experimental bond lengths of the studied structures (Table 1), although the specific values were not critical within certain ranges. Excessively large bond lengths failed in stabilizing the singlet ground state. The calculated axial ligand induced splitting for the asymmetric case (the differences with the symmetric one being small) is 50 cm^{-1}. It is clear from this result that within the present level of calculation (see discussion below) this effect cannot be neglected. As the axial ligands are essential to stabilize the calculated ground state, all calculations presented below include them, so in all cases the Q-band splitting will present an axial ligand contribution that cannot be separated from other effects.

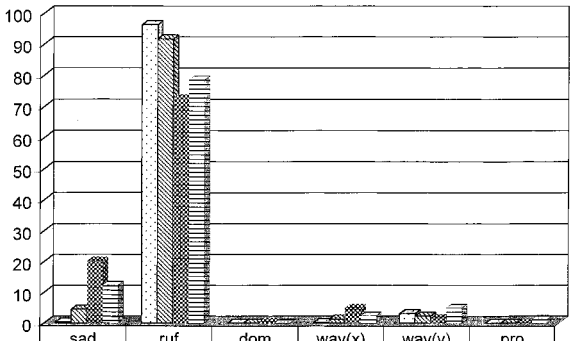

	sad	ruf	dom	wav(x)	wav(y)	pro
□ c552	0.37	96.2	0.06	0.23	3.1	0.02
▨ horse heart	4.52	91.6	0.04	1.34	2.36	0.04
※ tuna heart	20.2	72.7	0.36	4.96	1.59	0.21
☰ yeast	12.4	78.6	0.09	2.5	5.08	1.37

Figure 3. Structural decomposition of the heme macrocycle used in this work. Each mode corresponds to the lowest frequency out of plane vibration normal mode of one of six irreducible representations of D_{4h}.

Macrocycle Conformation. In cytochrome *c*, the porphyrin ring is covalently bonded to the protein by two cysteine residues. As shown by Jentzen et al.,[35] the peptide sequence between and including the cysteine residues linking the heme to the protein is correlated with the macrocycle conformation, suggesting that the protein exerts strains on the porphyrin ring that are relieved by adopting a nonplanar conformation. This conformation can be expressed in a quantitative way through a projection of the macrocycle structure on the lowest frequency out of plane normal modes of vibration (a minimal basis set of six 24-dimensional vectors). Following the work of Jentzen et al.[36] we calculate the normal modes components for the four structures used in this work, and these results are shown in Figure 3 expressed as percent contribution to the total structure. In all cases the conformation presents a high degree of ruffling, the main difference between c_{552} and the other proteins is its almost pure ruffled conformation, while in the others some appreciable saddled contribution is observed. We show also in Table 1 the root-mean-square deviations of the macrocycle atoms from the mean plane (a measure of the nonplanarity) and the root mean in-plane square deviation of the structures from a reference symmetric macrocycle, as defined in Jentzen et al.[36] To correlate the effect of nonplanar conformation with the Q-band splitting, we have to consider if the experimental splitting observed is compatible with the degree of nonplanarity of the structures and, as conformation is almost conserved through the series studied, if the different observed splittings are compatible with differences in conformation. We take the heme coordinates from the pdb files for the four structures, including axial ligands as explained above and substitute peripheral substituents with hydrogen. We calculate electronic spectra for these structures, the results reflect the conformation contribution to the spectra (superposed with the axial ligand contribution). The calculated splittings are shown in the second column of Table 2. As can be seen, the quantitative agreement with experimental results is poor, but the results suggest that there is effectively a contribution from macrocycle conformation to the spectral splitting of the Q-band. The differences obtained for the structures are greater than one might expect from examining the normal mode conformational analyses presented in Figure 3. This is associated with the fact that the normal mode decomposition, depending on the position of all atoms, may not be sensitive to the deviation of a single atom from a more stable position, while the quantum chemical calculation can be strongly influenced by this. This is particularly true in methods as the one used here, with a minimal basis set for the atomic orbitals.

Peripheral Substituents. Peripheral substituents can modify the electronic spectra of the porphyrin macrocycle by affecting the molecular orbitals involved in the electronic transitions. For most substituents this effect should be small. In cytochrome *c*, the propionates, with a relatively high charge density, although separated by four bond lengths from the macrocycle can affect the polarizable p orbitals. This results in a permanent dipole moment of the heme group and a break of symmetry. The effect of propionates was accounted for in previous work through considering their contribution to the electrostatic field. In this work we include all the peripheral substituents explicitly in the quantum chemical calculation, except the covalent bonds to the protein that were substituted with methyl groups. The results of this calculation for each of the structures is presented in Table 2, column 3. The effect on the calculated splitting is of the order of magnitude of the observed ones and is different for each structure. For yeast cytochrome *c* and horse heart cytochrome *c* the splitting is reduced with respect to the value with no propionates while for the two other structures is increased.

Electrostatic Field. The influence of electrostatic fields on heme spectra was discussed in previous works and summarized in the Introduction.

As we include the heme-propionates explicitly in the quantum chemical calculation, we were able to appreciate better the effect of the rest of the protein in the spectra. With the charge sets discussed in the computational modeling section, and the whole structure (axial ligands, propionates, nonplanar conformation) we obtained the splitting that are shown in the last column of Table 2. The external electrostatic field increases the splitting for the horse heart, tuna heart cytochrome *c* and cytochrome c_{552} and decrease it for yeast cytochrome *c*. We did not find significant differences in the calculated electrostatic fields patterns for the four structures. This suggests that the different effect on the splitting should arise from a combination of all the effects.

IV. Conclusions

The results obtained show, that at this level of calculation the contributions to the spectral splitting of the Q-band of the different factors that lower the symmetry of the heme group (macrocycle conformation, axial ligands, peripheral substituents and electrostatic field) are of the same order of magnitude. Our calculations (except for the symmetric model reference) use the coordinates as obtained from the X-ray structure files. Because of the limitations of a minimal basis set for quantum chemical calculations to treat highly distorted structures, relatively small errors within the precision of the X-ray structure determination can induce nonnegligible differences in our results. More relaxed structures can be obtained from a previous molecular mechanics minimization. As there is no clear correlation between the existing heme force fields and the quantum chemical methods used in this work, the quantitative improvement of this approach will be limited. An alternative approach will be the use of heme structures obtained as result of quantum chemical energy minimization. For this to improve the results showed in this paper, those calculations should be done with ab initio methods and with extended basis. As the actual conformation adopted by the heme depends on all factors discussed above, they should be included in the calculation to achieve good results. Besides the difficult task of including the protein-induced conformation of the macrocycle, the use of extensive configuration interaction will be lost. This represents a complex problem in its own and will be the subject of future work.

Despite the limitations mentioned above, our results show clearly that the Q-band splitting arises from a delicate balancing between the factors responsible of symmetry reduction. Within the degree of accuracy of the calculations and the experimental structural data, there is no clear correlation between structure and degree of splitting, in the sense that given a certain structure no prediction can be made on the expected experimental splitting. This reflects not only the limited precision achievable in the calculations and experimental structural data but also the limited set of structures in which experimental data is available. In this work we proposed a systematic way of analyzing experimental results, and we believe that this method applied to a large set of experimental data will allow one to obtain correlations between structure and Q-band splitting.

Acknowledgment. The National Institute of Health grant PO1 GM48310, RO1 GM55004 and RO1 GM 35342 supported this work. We thank Dr. Eric Manas for helpful discussions.

References and Notes

(1) Loew, G. H. *Iron Porphyrin*; Addison-Wesley: Reading, MA, 1983; Vol. 1, pp 1−87.
(2) Scheidt, W. R.; Reed, C. A. *Chem. Rev.* **1981**, *81*, 543−555.
(3) Makinen, M. W.; Churg, A. K. *Iron Porphyrins*; Addison-Wesley: Reading, MA, 1983; pp 141−235.
(4) Gouterman, M. *The Porphyrins*; Academic Press: New York, 1978; pp 1−156.
(5) Reddy, K. S.; Angiolillo, P. J.; Wright, W. W.; Laberge, M.; Vanderkooi, J. M. *Biochemistry* **1996**, *35*, 12820−12830.
(6) Balog, E.; Kis-Petik, K.; Fidy, J.; Kohler, M.; Friedrich, J. *Biophys. J.* **1997**, *73*, 397−405.
(7) Wagner, G. C.; Kassner, R. J. *Biochem. Biophys. Res. Commun.* **1975**, *63*, 385−391.
(8) Keilin, D.; Hartree, E. F. *Nature* **1949**, *164*, 254−259.
(9) Friedman, J. M.; Rousseau, D. L.; Adar, F. *Proc. Natl. Acad. Sci. U.S.A.* **1977**, *74*, 2607−2611.
(10) Ahn, J. S.; Kitagawa, T.; Kanematsu, Y.; Nishikawa, Y.; Kushida, T. *J. Lumin.* **1995**, *64*, 81−86.
(11) Shelnutt, J. A. *J. Chem. Phys.* **1980**, *72*, 3948−3958.
(12) Schweingruber, M. E.; Sherman, F.; Stewart, J. W. *J. Biol. Chem.* **1977**, *252*, 6577−6580.
(13) Wilson, D. F. *Arch. Biochem. Biophys.* **1967**, *121*, 757−768.
(14) Hagihara, B.; Oshino, R.; Iizuka, T. *J. Biochem.* **1974**, *75*, 45−51.
(15) Manas, E. S.; Wright, W. W.; Sharp, K. A.; Friedrich, J.; Vanderkooi, J. M. *J. Phys. Chem. B.* **2000**, *104*, 6932−6941.
(16) Cowan, J. A.; Gray, H. B. *Inorg. Chem.* **1989**, *28*, 4554−4556.
(17) Manas, E.; Vanderkooi, J. M.; Sharp, K. *J. Phys. Chem. B* **1999**, *103*, 6334−6348.
(18) Gouterman, M. *J. Chem. Phys.* **1959**, *30*, 1139−1161.
(19) Fee J. A.; Chen, Y.; Todaro, T. R.; Bren, K. L.; Patel, K. M.; Hill, M. G., Gomez-Moran, E.; Loehr, T. M.; Thony-Meyer, J. Ai. L.; Williams, P. A. Stura E.; Sridhar V.; McRee D. E. *Protein Sci.*, in press.
(20) Tinai, K.; Ericsson, H. H.; Hon-nami, K.; Miyaza, T. *Biochem. Biophys. Res. Commun.* **1985**, *128*, 781−787.
(21) Than, M. E.; Hof P.; Huber, R.; Bourenkov, G. P.; Bartunik, H. D.; Buse, G.; Soulimane, T. *J. Mol. Biol.* **1997**, *271*, 629.
(22) Bacon, A. D.; Zerner, M. C. *Theor. Chim. Acta* **1979**, *53*, 21−54.
(23) Ridley, J.; Zerner, M. C. *Theor. Chim. Acta* **1973**, *32*, 111−134.
(24) Ridley, J. E.; Zerner, M. C. *Theor. Chim. Acta* **1976**, *42*, 223−236.
(25) Nicholls, A.; Honig, B. *J. Comput. Chem.* **1991**, *12*, 435−445.
(26) Jayaram, B.; Sharp, K. A.; Honig, B. *Biopolymers* **1989**, *28*, 975−993.
(27) Gilson, M.; Sharp, K.; Honig, B. *J. Comput. Chem.* **1988**, *9*, 327−335.
(28) Sharp, K.; Honig, B. *Annu. Rev. Biophys. Chem.* **1990**, *19*, 301−332.
(29) Warshel, A.; Aqvist, J. *Annu. Rev. Biophys. Biophys. Chem.* **1991**, *20*, 267−298.
(30) Bushnell, G. W.; Louie, G. V.; Brayer, G. D. *J. Mol. Biol.* **1990**, *214*, 585−595.
(31) Takano, T.; Dickerson, R. E. *J. Mol. Biol.* **1981**, *153*, 79−94 (95−115).
(32) Louie, G. V.; Brayer, G. D. *J. Mol. Biol.* **1990**, *214*, 527−555.
(33) Hon-Nami, K.; Oshima, T. *J. Biochem.* **1977**; 82; 769−776.
(34) Edwards, W. D.; Weiner, B.; Zerner, M. C. *J. Am. Chem. Soc.* **1986**, *108*, 1309−1321.
(35) Jentzen, W.; Ma, J.-G.; Shelnutt, J. A. *Biophys. J.* **1998**, *74*, 753−763.
(36) Jentzen, W.; Song, X.-Z.; Shelnutt, J. A. *J. Phys. Chem. B* **1997**, *101*, 1684−1699.